Discrepancies in simulated ocean net surface heat fluxes over the North Atlantic

Article

Accepted Version

Liu, C., Yang, Y., Liao, X., Cao, N., Liu, J., Ou, N., Allan, R. P. ORCID: https://orcid.org/0000-0003-0264-9447, Jin, L., Chen, N. and Zheng, R. (2022) Discrepancies in simulated ocean net surface heat fluxes over the North Atlantic. Advances in Atmospheric Sciences, 39 (11). pp. 1941-1955. ISSN 0256-1530 doi: 10.1007/s00376-022-1360-7 Available at https://centaur.reading.ac.uk/104694/

To link to this article DOI: http://dx.doi.org/10.1007/s00376-022-1360-7

Publisher: Springer

Discrepancies in simulated ocean net surface heat fluxes over the North Atlantic

Journal:	*Advances in Atmospheric Sciences*
Manuscript ID	AAS-2021-0360.R2
Manuscript Type:	Original Article
Date Submitted by the Author:	11-Jan-2022
Complete List of Authors:	Liu, Chunlei; Guangdong Ocean University; Guangdong Ocean University; University of Reading, Department of Meteorology Yang, Yazhu; Guangdong Ocean University; Guangdong Ocean University; Guangdong Ocean University Liao, Xiaoqing; Guangdong Ocean University; Guangdong Ocean University; Guangdong Ocean University Cao, Ning; Guangdong Ocean University; Guangdong Ocean University; Guangdong Ocean University Liu, Jimmy; University of Cambridge, Department of Mathematics Ou, Niansen; Guangdong Ocean University; Guangdong Ocean University; Guangdong Ocean University Allan, Richard; University of Reading, Department of Meteorology Jin, Liang; Guangdong Ocean University; Guangdong Ocean University; Guangdong Ocean University Chen, Ni; Guangdong Ocean University; Guangdong Ocean University; Guangdong Ocean University Zheng, Rong; Guangdong Ocean University

Discrepancies in simulated ocean net surface heat fluxes over the North Atlantic

Chunlei Liu[1,2,5], Yazhu Yang[1,2,3], Xiaoqing Liao[1,2,3], Ning Cao[*1,2,3], Jimmy Liu[4],

Niansen Ou[1,2,3], Richard P. Allan[5,6], Liang Jin[1,2,3], Ni Chen[1,2,3], Rong Zheng[1,2,3]

[1] *South China Sea Institute of Marine Meteorology, Guangdong Ocean University, Zhanjiang, China*

[2] *CMA-GDOU Joint Laboratory for Marine Meteorology, Guangdong Ocean University, Zhanjiang, China*

[3] *College of Ocean and Meteorology, Guangdong Ocean University, Zhanjiang, China*

[4] *Department of Mathematics, Trinity College, University of Cambridge, UK*

[5] *Department of Meteorology, University of Reading, Reading RG6 6BB, UK*

[6] *National Centre for Earth Observation, Reading, UK*

---

*Corresponding authors : Ning Cao
Email: ncao@gdou.edu.cn

ABSTRACT

The change in ocean net surface heat flux plays an important role in the climate system. It is closely related to the ocean heat content change and ocean heat transport, particularly over the North Atlantic, where the ocean loses heat to the atmosphere, affecting the AMOC (Atlantic Meridional Overturning Circulation) variability and hence the global climate. However, the difference between simulated surface heat fluxes is still large due to poorly represented dynamical processes involving multiscale interactions in model simulations. In order to explain the discrepancy of the surface heat flux over the North Atlantic, data sets from nineteen AMIP6 and eight *highresSST-present* climate model simulations are analyzed and compared with the DEEPC (Diagnosing Earth's Energy Pathways in the Climate system) product. As an indirect check of the ocean surface heat flux, the oceanic heat transport inferred from the combination of the ocean surface heat flux, sea ice and ocean heat content tendency is compared with the RAPID (Rapid Climate Change-Meridional Overturning Circulation and Heat flux array) observations at 26°N in the Atlantic. The AMIP6 simulations show lower inferred heat transport due to less heat loss to the atmosphere. The heat loss from the AMIP6 ensemble mean north of 26°N in Atlantic is about 10 Wm^{-2} less than DEEPC, and the heat transport is about 0.30 PW lower than RAPID and DEEPC. The model horizontal resolution effect on the discrepancy is also investigated. Results show that by increasing the resolution, both surface heat flux north of 26°N and heat transport at 26°N of the Atlantic can be improved.

Key words: Ocean net surface heat flux, ocean heat transport, discrepancy, simulations, observations https://doi.org/10.1007/s00376-022-1360-7

Article Highlights:

- Surface heat loss from the AMIP6 ensemble mean north of 26°N in the Atlantic is about 10 Wm^{-2} less than the observation.
- Area mean surface heat loss north of 26°N in the Atlantic increases by 5.5 Wm^{-2} per degree increase in horizontal resolution.
- The resolution dependence of the net surface heat flux is primarily related to the latent heat flux component.

1. Introduction

The ocean net surface heat flux (F_S) determines how much energy enters the ocean. It is an indicator of the Earth's energy budget imbalance, since about 84%-93% of the excess energy entering the Earth system has accumulated in the ocean (Cheng et al., 2017; von Schuckmann et al., 2016, 2020; Cuesta-Valero et al., 2021), due to the small heat capacity of the atmosphere and upper layer soil. Regionally, F_S is also closely related to the oceanic heat transport which affects regional climates (Caesar et al., 2021) and the inter-tropical convergence zone (Donohoe et al., 2013; Frierson and Hwang, 2012; Kang et al., 2018). Therefore, accurate estimation of F_S is essential for understanding current climate change and its projections.

The F_S from both climate model simulations and atmospheric reanalyses has large discrepancies (Liang and Yu, 2016; Josey et al., 2013). The varying subgrid scale parameterizations, the spatially and temporally unevenly distributed samplings of *in situ* measurements, the near-surface air temperature and humidity that cannot be directly retrieved from satellites, and changes related to the observational systems can all introduce a great number of uncertainties to the F_S estimations (Yu et al., 2013). So far, the F_S estimated from the residual of the net TOA (Top of the Atmosphere) radiative flux minus the accumulated total column atmospheric energy tendency and divergence has been widely used in the community (Trenberth et al., 2019). This residual method can ensure the energy conservation of the entire atmospheric column. Much progress in applying the energy budget residual method has been made in recent years using data from atmospheric reanalyses (Mayer and Hamburger, 2012; Trenberth, 1991; Mayer et al., 2017, Liu et al., 2015, 2017, 2020). The mass correction has been applied to the reanalysis data because of mass conservation issues leading to spurious wind divergences associated with the data assimilation process (Mayer and Hamburger, 2012; Trenberth, 1991). A recent study (Mayer et al., 2017) showed that the enthalpy of the atmospheric water vapor should also be accounted for to avoid inconsistencies arising from the non-zero atmospheric lateral total (dry plus moist) mass flux divergence, which balances surface freshwater flux (i.e. precipitation minus evaporation). These inconsistencies are particularly large when using the Kelvin temperature scale that is common in atmospheric science. However, the inferred multiannual global land area mean net surface flux (F_{SL}) is still not realistic from the residual method after these treatments, so the deficit/excess of the F_{SL} needs to be further adjusted based on land surface energy budget considerations and redistributed to the oceans (Liu et al., 2015, 2017, 2020). The results after the F_{SL} adjustment showed improved consistency with buoy data (Liu et al., 2017) and other observations (Mayer et al., 2021b).

The energy budget over the North Atlantic plays an important role in the climate system, since it is related to the atmospheric and oceanic heat transports from the low latitudes to the high latitudes (Hirschi et al., 2019), influencing the Atlantic Meridional Overturning Circulation (AMOC) and the pronounced warming trend in Arctic in recent decades, which is stronger than the global average warming near the surface (Serreze and Barry, 2011). The surface heat loss to the atmosphere in the North Atlantic can affect the climate in western Europe and even in Eurasia (Rahmstorf and Ganopolski, 1999).

Direct observations of ocean surface fluxes are rare. There are only some limited sectional measurements of ocean heat transport in the North Atlantic. The most well-known of these is the RAPID (Rapid Climate Change-Meridional Overturning Circulation and Heat flux array) observations at 26°N across the Atlantic (Smeed et al., 2017), which can be used as anindirect check of the ocean net surface heat fluxes (Trenberth et al., 2019; Liu et al., 2017, 2020). In order to investigate the discrepancies of the ocean net heat flux over the North Atlantic, ocean net surface heat fluxes from AMIP6 (Atmospheric Model Intercomparison Project Phase 6) and the *HighresSST-present* experiment (Eyring et al., 2016) arecompared with those from the DEEPC (Diagnosing Earth's Energy Pathways in the Climate system) product estimated from the residual method, using the recently-released ERA5 (the fifth generation ECMWF ReAnalysis) atmospheric reanalysis (Hersbach et al., 2020). The inferred oceanic heat transport iscompared with RAPID observations and the effect of model horizontal resolution on the discrepancy assessed. Data and methods are described in section 2, Results are shown in section 3 and section 4 presents discussions and conclusions.

2. Data and methods

The F_S estimated from observations is based on the energy budget residual method, which is the net TOA radiative flux minus the accumulated total column atmospheric energy tendency and divergence (Trenberth and Solomon, 1994; Mayer and Haimberger, 2012; Liu et al., 2015, 2017). The high-quality TOA radiative fluxes are from CERES (Clouds and the Earth’s Radiant Energy System) from March 2000 (Loeb et al., 2012; Kato et al., 2013) to the present. The TOA fluxes since 1985 prior to CERES have been reconstructed by Liu et al. (2020), following the procedure of Allan et al. (2014) with some modifications. The climatology for the reconstructed TOA flux is from CERES and anomalies are from ERA5 (Hersbach et al., 2020) constrained by ERBE WFOV (Earth Radiation Budget Experiment Satellite wide field of view, 72-day mean, Wong et al., 2006) anomalies at 10° × 10° resolution to representthe observed spatial and temporal variability.

Discontinuities in the reconstruction were dealt with using an ensemble of AMIP6 simulations. The global mean OHCT (ocean heat content tendency) and net TOA flux have been compared. The general agreement in both the absolute value and variability between them suggests the robustness of the reconstruction over 1985–1999 (Liu et al. 2020).

The mass corrected total atmospheric energy divergence (TEDIV) has been calculated by Mayer et al (2021a) from the recently-released ERA5 atmospheric reanalysis, with 137 model levels and a horizontal resolution of 0.25°×0.25°. The land surface flux adjustment has been applied to the mass corrected TEDIV to estimate F_S, as described in detail by Liu et al. (2017, 2020). The inferred global mean ocean net surface heat flux of 1.7 Wm^{-2} (over 1985–2018) agrees well with recent observation based estimates from von Schuckmann et al. (2020) to within 1 Wm^{-2}, which is substantially better compared to model- and satellite-based estimates (Mayer et al., 2021a). For example, CERES+OAFlux (Objectively Analyzed air-sea Fluxes, Yu and Weller, 2007) has an ocean mean of ~28 Wm^{-2} for 60˚N–60˚S, and simulated fluxes from ERA5 model forecasts exhibit an ocean mean of ~6 Wm^{-2}. JRA55 (the Japanese 55 year reanalysis, Kobayashi et al., 2015) ocean mean heat flux is -17 Wm^{-2} and MERRA2 (Modern-Era Retrospective analysis for Research and Applications, Version 2, Gelaro et al., 2017) ocean surface heat flux has a mean of -5 Wm^{-2} (Cronin et al., 2019). The inferred ocean heat transport of 1.23 PW (over the RAPID period) is very close to the RAPID observation of 1.22 PW at 26˚N of Atlantic, much better than 0.66 PW inferred from the ERA-Interim surface flux (Liu et al., 2020).

Based on Loeb et al. (2016) and Trenberth and Fasullo (2017), the ocean heat divergence ($\nabla{\cdot}E_O$) in a water column can be calculated by

$$\nabla \cdot E_O = F_O - OHCT \qquad (1)$$

where $F_O = F_S - F_{ice}$ is the energy entering the ocean, F_{ice} is the energy associated with sea ice formation and melting and is calculated from five ensemble members of ECMWF's ORAS5 (Ocean ReAnalysis System 5) reanalysis (Zuo et al., 2019). OHCT is calculated from OHC (Ocean Heat Content) using central differences, e.g. the OHCT in February is the difference of OHCs between March and January and divided by the time difference. The OHCT calculated by Liu et al. (2020) using the OHC integrated over 0–2000 m is used in this study, since it shows good agreement in both absolute value and variability with the global mean F_S. The ORAS5 is a state-of-the-art eddy-permitting ocean reanalysis running on ¼° resolution. The ORAS5 has been validated and it is found to provide realistic variability in ocean heat storage and oceanic transports in the tropics (Mayer et al., 2018; Trenberth and Zhang, 2019) and the Arctic (Uotila et al., 2019; Mayer et al., 2019). Considering that the oceanic heat transport is zero at the boudary and the heat transport through the Bering Strait is small and can be neglected (Koenigk and Brodeau, 2014), the oceanic heat transport at different latitudes in the North Atlantic can be accurately estimated by integration from the North Pole.

The AMIP6 and high resolution *highresSST-present* climate model simulations have prescribed observed sea surface temperature (SST) and sea ice and realistic radiation forcings (Eyring et al., 2016). The *highresSST-present* is defined in the framework of HighResMIP (Haarsma et al., 2016) and a configuration available in the CMIP6 archive similar to AMIP6, but with a higher horizontal resolution. The *highresSST-present* experiment is designed to allow for an evaluation of the sensitivity of climate model output to spatial resolution, and to help understand the origins of model biases. The net surface fluxes from these model simulations are calculated by summing up four components of surface latent heat flux, sensible heat flux, shortwave and longwave radiative fluxes. There are nineteen AMIP6 models and eight *highresSST-present* models used in this study. Unless stated otherwise, the AMIP6 data include both normal AMIP6 and *highresSST-present* simulations. The data sets used in this study are listed in Table 1, with brief descriptions.

3. Results

The multiannual mean (2006-2013) of ocean net surface heat fluxes in the North Atlantic from DEEPC, ERA5 and AMIP6 (including *highresSST-present*) are plotted in Figs. 1a-c. It can be seen that in general the North Atlantic loses heat to the atmosphere, particularly over the Gulf Stream and the high latitude.This loss is compensated by the oceanic heat transport from the low latitude to the high latitude in the Atlantic. The corresponding zonal means are plotted in Fig. 1d. The shaded area is the AMIP6 ensemble mean ± one standard deviation (STD). The maximum heat loss is at 39°N where the heat fluxes are 71, 66 and 63 Wm^{-2} from DEEPC, ERA5 and the AMIP6 ensemble mean, respectively. The DEEPC data show more heat loss than the AMIP6 ensemble mean north of 35°N, implying more oceanic heat transport is needed to compensate this loss.

The differences in Fig. 1e (ERA5 minus DEEPC) and Fig. 1f (AMIP6 minus DEEPC) show similar large discrepancies over the mid-high latitudes. However, it must be borne in mind that the AMIP6 models have prescribed observed SST and sea ice and realistic radiative forcings; therefore the atmospheric internal component of F_S is mostly removed when taking the ensemble mean, which is primarily the atmospheric response to the prescribed forcings. Meanwhile, the F_S from the DEEPC product includes both the atmospheric internal component and the atmospheric response to the prescribed forcings;

thus, the F_S difference between DEEPC and the AMIP6 ensemble mean may not indicate the discrepancy of F_S between them, but may be largely due to the atmospheric internal component of F_S, which was found to be critical in forcing the oceanic variability in the mid-high-latitude North Atlantic (Barsugli and Battisti, 1998; Delworth and Greatbatch, 2000; Dong and Sutton, 2002; Kwon and Frankignoul, 2012; Colfescu and Schneider, 2020; Chen, et al., 2021). However, after checking the difference between DEEPC and individual AMIP6 models, spatial patterns similar to Figs. 1e and 1f are found (not shown).

The large discrepancy region also displaysa large STD of the AMIP6 ensemble, as shown in Fig. 1g, except that around the Arctic region where F_S is constrained to be close to zero. The STD along the western boundary current, such as in the slope regions of the Greenland Ocean and in the Gulf Stream, is large because of the intense mesoscale activity there (Putrasahan et al., 2013, Chelton and Xie, 2015; Roberts et al., 2017). The ocean eddy activity will affect the turbulent heat fluxes (Roberts et al., 2016), but it cannot be well represented by the prescribed SST over these regions. The zonal mean in Fig. 1h shows that the mean heat loss from DEEPC between 50-75°N is about 15 Wm^{-2} more than that from ERA5 and 13 Wm^{-2} more than simulated by the AMIP6 ensemble mean. The difference between DEEPC and the individual AMIP6 model is also examined (not shown) and it is found that 74% (20 out of 27 models) of these models show differences between 9-25 Wm^{-2} over 50-75°N. The mean STD of the AMIP6 net surface heat flux over 50-75°N is about 12 Wm^{-2}. The heat loss averaged over the region north of 26°N from the AMIP6 ensemble mean is about 10 Wm^{-2} less than that from DEEPC, and the STD of the diffence between DEEPC and individual AMIP6 model is about 4.3 Wm^{-2}. The deseasonalized time series of the area mean ocean net surface heat flux north of 26°N is plotted in Fig. 2. Both DEEPC and the AMIP6 ensemble mean show more-or-less consistent decadal variability after 1995, such as the decrease over 2002-2008 and the increase after 2010. The DEEPC estimate does not have a significant trend, but the AMIP6 ensemble mean has a significant trend of -0.34 Wm^{-2}/decade. The inferioragreement in the interannual variability between DEEPC and the AMIP6 ensemble mean is partly due to the aforementioned atmospheric internal component of F_S. Different horizontal resolutions of AMIP6 models may also play an important role and will be further discussed below. AMIP6 models have prescribed sea ice, but in the real world the sea ice at high latitudes can not only insulate and impede the heat loss from the ocean to the atmosphere, but also can alter the water salinity by the brine rejection during the sea ice formation, therefore increasing the water density and influencing the AMOC and ocean current (Jansen, 2017), affecting the turbulent fluxes. The variability of ERA5 shows less consistency with DEEPC and the AMIP6 ensemble mean, mainly due to the imbalance of the wind-induced mass transport and surface pressure changes, which arises from the lack of observational constraint on divergent winds (Trenberth et al. 2009; Mayer and Haimberger 2012; Liu et al. 2015, 2020).

As an indirect check of the ocean net surface heat fluxes in the North Atlantic, the multiannual mean (2006–2013) meridional heat transport is integrated from the North Pole using equation (1) from different data sets of net surface heat fluxes, including the DEEPC, ERA5, nineteen AMIP6 and eight *highresSST-present* climate model simulations. The sea ice and OHCT are from the ORAS5 ocean reanalysis. The results are shown in Fig. 3. Grey lines are the heat transport from individual AMIP6 simulations and the ensemble mean is the solid black line. The vertical dashed red line shows the location of 26°N. It can be seen that the transport from most of the AMIP6 members is lower than that inferred from DEEPC in the north of 26°N. Only one member has the heat transport compatible with the DEEPC, implying that the area mean F_S from AMIP6 in the north of 26°N is higher than the estimated DEEPC product, i.e. less heat loss. The inferred AMIP6 ensemble mean oceanic heat transport in the Atlantic is comparable with that inferred from the direct ERA5 surface fluxes in the north of 26°N, but is much lower than that of DEEPC. The heat transport from AMIP6 spreads quickly after starting the integration from the North Pole, indicating the large spread of the simulated F_S in the North Atlantic, since both F_{ice} and OHCT are all from the ORAS5. The AMIP6 ensemble mean is closer to DEEPC in the southern hemisphere, but it is still about 0.3-0.4 PW lower. The oceanic heat transport inferred from direct ERA5 surface heat flux in the southern hemisphere is nearly at the lower end of that from the AMIP6.

The time series of the oceanic heat transport at 26°N is plotted in Fig. 4. The inferred heat transport from DEEPC shows reasonable agreement with the RAPID observation in both variability and quantity. The correlation coefficient over the RAPID period (April 2004 to February 2017 in this study) is 0.32 and the mean heat transports are 1.21 PW for RAPID and 1.24 PW for DEEPC, respectively. The earlier trend of RAPID data from 2006–2008 is subject to greater uncertainty in observations (Trenberth et al. 2019; Trenberth and Fasullo 2018). The variability agreement is better after 2008 and the correlation coefficient is 0.73 over 2008-2016. The transport inferred directly from the ERA5 surface heat fluxes is much lower than that from DEEPC, even though it is higher than that from ERA-Interim, which is about 0.66 PW over 2004-2016 (Liu et al., 2020). There is good agreement in both the variability and quantity of the heat transport between the AMIP6 ensemble mean and ERA5.The correlation coefficient is 0.66 and the mean transports are all 0.91 PW over 1985-2014. The correlation coefficient between DEEPC and AMIP6 is 0.73 over the same period.

The spread of F_S is large between AMIP6 model simulations because of different subgrid scale parameterizations in the model dynamics, such as the cumulus convection, cloud microphysics, turbulence, radiation and land-surface processes. However, the model resolution may play a role. The resolution effects on the multiannual (2006-2013) area mean F_S over the globe and the ocean area north of 26°N Atlantic are plotted in Fig. 5a and 5b, respectively. The effect on the oceanic heat transport at 26°N is plotted in Fig. 5c. Fig. 5a shows the decrease of the global area mean F_S with the increase of the model grid point distance. Model 5 (CanESM) behaves differently. The regression slopes are $\boldsymbol{m}$=-1.57±1.40 and $\boldsymbol{m}$=-0.48±1.21 Wm^{-2} per degree horizontal resolution without and with model 5 counted, respectively. The correlation coefficients between the F_S and latitudinal resolution are $\boldsymbol{r}$=-0.43 and -0.16 without and with model 5 counted, respectively. For the region north of 26°N Atlantic, the heat loss increases with the increase of the model resolution. The regression slopes are $\boldsymbol{m} = 5.47 \pm 3.56$ and $\boldsymbol{m} = 3.63 \pm 2.88$ Wm^{-2} per degree resolution without and with model 5 counted, respectively. The influence of model 5 on F_S north of 26°N is not as large as that for the global mean. The corresponding correlation coefficients between the mean F_S north of 26°N and the latitudinal resolution are $\boldsymbol{r}$=0.54 and 0.46 respectively. Based on equation (1), it is expected that the relationship between F_S and model resolution should be the opposite of that between the oceanic heat transport and the resolution. This is shown in Fig. 5c. The heat transport at 26°N increases with the increasing model resolution. The regression slopes are $\boldsymbol{m} = -0.22 \pm 0.13$ and $\boldsymbol{m} = -0.15 \pm 0.10$ PW per degree resolution without and with model 5 counted and the corresponding correlation coefficients between the heat transport at 26°N and the latitudinal resolution are ***r***=-0.59 and -0.52, respectively. It is observed that when the model resolution is high enough, the heat transport can be compatible with that inferred from DEEPC products.

To investigate the causes of the resolution dependence of F_S in the global mean and north of 26°N inthe Atlantic, the dependence of flux components at TOA and surface on the resolution has been plotted in Fig. 6. For global mean TOA radiative fluxes, the RSW (Reflected Shortwave Radiation) decreases with increasing resolution (Fig. 6a), but more OLR (Outgoing Longwave Radiation) leaves the TOA to compensate it to some extent (Fig. 6b). The net effect is that the radiation flux entering the TOA (F_T) increases with higher resolution (Fig. 6c). These results are consistent with Vanniere et al. (2019) using a different set of climate models. Due to the small atmospheric heating capacity and no horizontal divergence for the global mean, most of the energy enetering the TOA will reach the surface. There is a strong correlation between F_T and F_S (Fig. 6d); therefore the global mean F_S also increases with the higher resolution (Fig. 5a). The physical processes leading to the global area mean RSW and OLR dependence on the model resolution are complicated due to the bias compensation between different regions (Moreno-Chamarro et al., 2021). The increase of OLR and the decrease of RSW with the higher model horizontal resolution are primarily due to a change of cloud radiative forcings in regions of mean ascending motion. Vanniere et al. (2019) suggested a possible explanation: at higher resolution, high intensity precipitation events are generated by more compact and more intense convective systems, thus reducing the mean cloud fraction. A more detailed analysis of cloud radiative properties is beyond the scope of this study but will be the object of a future study.

For the F_S in the region north of 26°N of the Atlantic, four flux components are assessed and it is found that the latent heat (*LH*) has similar resolution dependence with the F_S as shown in Fig. 6e. Fig. 6f shows the scatter plot between the area mean F_S and *LH* (both over the north of 26°N in the Atlantic). The same range for both axes are selected, so the contribution of *LH* change to F_S change can be clearly seen. The increase of the surface evaporation with resolution has been reported by Vanniere et al. (2019) and is a global feature. One possible cause is the increase of SW radiation at surface due to the reduction of the mean cloud fraction (Demory et al., 2014). However, as the sea surface temperature is prescribed in AMIP6 simulations, it cannot mediate the increase of incoming shortwave to the surface latent heat flux. Another possible cause is the result of stronger surface wind speed (Terai et al., 2018), which will affect the relative motion between the wind at 10 m and the ocean surface current, and influence the turbulent heat fluxes based on the bulk formula. The sea ice drift at the high latitude can also influence the relative motion in the ocean surface and hence the surface heat flux. Therefore, the ocean surface wind and the sea ice drift may also play a role contributing to the discrepancy of the ocean surface heat flux as show in previous studies (Wu et al., 2017; Wu et al., 2021). Additionally, high-frequency atmospheric activity such as storms also can contribute to the discrepancy in the simulated ocean net surface heat flux (Condron and Renfrew, 2013; Holdsworth and Myers, 2015; Wu et al., 2016; Wu et al., 2020). More dedicated studies would be needed to conclude on the mechanism causing the increase of *LH* with resolution across models (Vanniere et al., 2019).

4. Discussion and conclusions

The North Atlantic net surface heat flux plays an important role in the climate system. It can affect the AMOC variation and climate change on the global scale. However, direct observations of F_S over the North Atlantic are sparse, therefore the estimated F_S from DEEPC using the residual method (Liu et al., 2020) has been used as the "truth" in this study. DEEPC products have been widely used in the community for climate research and model validation (Allison et al., 2020; Mayer et al., 2021a, b; Williams et al., 2015; Valdivieso et al., 2015; Senior et al., 2016; Roberts et al., 2016; Roberts et al., 2017; Hyder et al., 2018; Mignac et al., 2018; Cheng et al., 2019; Trenberth et al., 2019; Bryden et al., 2019). The latest DEEPC (version 5) product uses the mass corrected total atmospheric energy divergence from the latest ECMWF release of ERA5 atmospheric reanalysis (Mayer et al 2021a). By combining with the sea ice data and OHCT from the ECMWF ORAS5 ocean reanalysis, the net heat flux entering the ocean (F_O) is estimated and the oceanic heat transport in the Atlantic is calculated.

AMIP6 data, including the *highresSST-present* data sets, have been widely used for climate research. The ocean net surface heat flux in the North Atlantic from AMIP6 is compared with the DEEPC product in this study to check the discrepancy. There is a large spread of net surface heat fluxes among AMIP6 models. The AMIP6 surface heat loss to the atmosphere is less compared with the DEEPC product (Fig. 1). The inferred oceanic heat transport in the Atlantic is calculated and compared with observations as an indirect check of the net surface heat flux. When integrated from the North Pole, heat transports from all AMIP6 models are lower than that from the DEEPC product between the North Pole and 26°N of the Atlantic, and the AMIP6 ensemble mean is close to that inferred from direct ERA5 surface heat fluxes. The integrated heat transport from AMIP6 spreads quickly, implying a large spread in zonal distribution of the net surface heat fluxes, as shown in Fig. 1h. The time series of the heat transport at 26°N across theAtlantic shows good agreement in variability and magnitudebetween DEEPC and RAPID observations. The mean heat transports are 1.21 PW for RAPID and 1.24 PW for DEEPC, respectively, over the RAPID observation period. The agreement in variability between them is better after 2008 and the correlation coefficient is 0.73 over 2008-2016. The inferred heat transports from AMIP6 and ERA5 agree with each other in terms of variability and magnitude, but they are all about 0.3 PW lower than the DEEPC observation-based estimate. It is noticed that the inferred heat transport from direct ERA5 surface heat fluxes is higher than that from ERA-Interim estimated by Liu et al. (2020).

The effect of model resolution on the net surface heat flux and heat transport has been investigated. Results show that the higher resolution did improve the agreement with observations of net surface heat fluxes over the area north of 26°N in the Atlantic, as well as the inferred heat transport. The global mean F_S increases with the increase of the resolution and the regression slope is about -1.57 Wm^{-2} per degree resolution, i.e. the higher the resolution, the higher the F_S. Further investigation found that the RSW decreases with increasing resolution (Fig. 6a), primarily due to a change of cloud radiative forcings in regions of mean ascending motion. Vanniere et al. (2019) suggested that at higher resolution, high intensity precipitation events are generated by more compact and more intense convective systems, thus reducing the mean cloud fraction. It merits a more detailed analysis and will be the objective of a future study. Since the atmospheric heat capacity is small, the global mean net TOA radiative flux F_T and net surface heat flux F_S are approximately balanced (Fig. 6d). Therefore, the global mean F_S will also increase with the higher model horizontal resolution.

The corrlation coefficient ***r***=0.54 between the area mean F_S north of 26°N in the Atlantic and the model horizontal resolution is significant using a two-tailed test and Pearson critical values at the 5% significance level. The regression slope is about 5.47 $\mathrm{Wm^{-2}}$ per degree resolution (Fig. 5b), implying more heat loss when the resolution is increased. Further investigation showed that the surface latent heat flux component displays similar resolution dependence to the regional total surface heat flux, F_S (Figs. 6e-f). One possible cause is the result of stronger surface wind speed (Terai et al., 2018), which will affect the relative motion between the wind at 10 m and the ocean surface current, and influence the turbulent heat fluxes based on the bulk formula. The sea ice drift at high latitudes can also influence the relative motion in the ocean surface and hence the surface heat flux. Therefore, the ocean surface wind and the sea ice drift may also contribute to the discrepancy of the ocean surface heat flux (Wu et al., 2017; Wu et al., 2021). Furthermore, high-frequency atmospheric activity such as storms also contribute to the discrepancy in the simulated net ocean surface heat flux (Condron and Renfrew, 2013; Holdsworth and Myers, 2015; Wu et al., 2016; Wu et al., 2020). AMIP6 models have prescribed the sea ice, but in the real world the sea ice at high latitudes can alter the water salinity by the brine rejection during the sea ice formation, therefore increasing the water density and influencing the AMOC and ocean current (Jansen, 2017), affecting the turbulent fluxes. More dedicated studies focusing on surface ocean processes and cloud radiative forcing should be conducted in the future (Vanniere et al., 2019).

As expected, the regression slope between the heat transport at 26°N and the resolution is about -0.22 PW per degree (Fig. 5c), indicating the higher the resolution, the greater the heat transport. The deviation of the AMIP6 heat transport from DEEPC and RAPID is also partly due to the difference in global mean net surface fluxes of AMIP6 simulations. However, the spread of the global area mean F_S is about 6.12 Wm^{-2}, while the F_S spread of 17.59 Wm^{-2} over the region north of 26°N in the Atlantic is much larger. Therefore, even when the global mean net surface fluxes from AMIP6 are constrained by the DEEPC product, the reduction in the spread of heat transport will be limited. This remains a challenge for the modelling community. In order to have a deep understanding of the discrepancy between model simulations and observations, further research is needed. These findings can help the research community more accurately interpret the historical simulations and projections produced by contemporary models. By using the ocean current and temperature from the coupled CMIP6 model simulations, the link between the ocean net surface heat fluxes and the oceanic heat transport can be further investigated.

Acknowledgements: This work is supported by the National Natural Science Foundation of China (42075036), Fujian Key Laboratory of Severe Weather (2021KFKT02) and the scientific research start-up grant of Guangdong Ocean University (R20001). Chunlei Liu is also supported by the University of Reading as a visiting fellow. Richard Allan is supported by the UK National Centre for Earth Observation grant NE/RO16518/1. The DEEPC data are available at http://www.met.rdg.ac.uk/~sgs01cll/DEEPC/, the RAPID data can be downloaded from https://rapid.ac.uk/rapidmoc/rapid_data/datadl.php, the ORAS5 from https://www.cen.uni-hamburg.de/icdc/data/ocean/easy-init-ocean/ecmwforas5.html and the AMIP6 data from https://esgf-node.llnl.gov/projects/cmip6/. We acknowledge all teams and climate modeling groups for making their data available.

References

Allan, R. P., C. Liu, N. B. Loeb, M. D. Palmer, M. Roberts, D. Smith, and P. L. Vidale, 2014: Changes in global net radiative imbalance 1985–2012. *Geophys. Res. Lett.*, **41**(15), 5588-5597, doi: 10.1002/2014GL060962.

Allison, L. C., M. Palmer, R. P. Allan, L. Hermanson, C. Liu, and D. M. Smith, 2020: Observations of planetary heating since the 1980s from multiple independent datasets. *Environ. Res. Commun.*, **2**(10), doi: 10.1088/2515-7620/abbb39.

Bao, Q., Y. Liu, G. Wu, and Coauthors, 2020: CAS FGOALS-F3-H and CAS FGOALS-F3-L Outputs for the High-Resolution Model Intercomparison Project Simulation of CMIP6. *Atmos. Ocean. Sci. Lett.*, **13**, 576-581, doi: 10.1080/16742834.2020.1814675.

Barsugli, J. J., and D. S. Battisti, 1998: The basic effects of atmosphere–ocean thermal coupling on midlatitude variability. *Journal of the Atmospheric Sciences*, 55, 477–493.

Boucher, O., and Coauthors, 2019a: Presentation and evaluation of the IPSLCM6A-LR climate model. *J. Adv. Model. Earth Syst.,* **12**(7), e2019MS002010, doi: 10.1029/2019MS002010.

Boucher, O., and Coauthors, 2019b: IPSL IPSL-CM6A-ATM-HR model output prepared for CMIP6 HighResMIP. *Earth System Grid Federation*. doi: 10.22033/ESGF/CMIP6.2361.

Boucher, O., and Coauthors, 2019c: IPSL IPSL-CM6A-LR model output prepared for CMIP6 HighResMIP. Earth System Grid Federation. doi: 10.22033/ESGF/CMIP6.13803.

Bryden, H. L, and S. Imawaki, 2001: Ocean heat transport. In: Siedler G, Church J, Gould J (eds) Ocean circulation and climate, Chap 6.2, Academic Press, London, pp 455–474.

Bryden, H. L., W. E. Johns, B. A. King, G. Mccarthy, E. L. Mcdonagh, B. I. Moat, and D. A. Smeed, 2019: Reduction in Ocean Heat Transport at 26°N since 2008 Cools the Eastern Subpolar Gyre of the North Atlantic Ocean. *J. Climate*, **33**(5), 1677-1689. doi: 10.1175/JCLI-D-19-0323.1.

Cao, J., B. Wang, Y. M. Yang, L. Ma, J. Li, B. Sun, Y. Bao, J. He, X. Zhou, and L. Wu, 2018: The NUIST Earth System Model (NESM) version 3: description and preliminary evaluation, *Geosci. Model Dev.*, **11**, 2975–2993, doi: 10.5194/gmd-11-2975-2018.

Caesar, L., G. D. McCarthy, D. J. R. Thornalley, N. Cahill and S. Rahmstorf, 2021: Current Atlantic Meridional Overturning Circulation weakest in last millennium. *Nature Geoscience,* **14**, 118–120, https://doi.org/10.1038/s41561-021-00699-z.

Colfescu, I., and E. K. Schneider, 2020: Decomposition of the Atlantic multidecadal variability in a historical climate simulation. *Journal of Climate*, **33**, 4229–4254.

Chen, H., E. K. Schneider, and Z. Zhu, 2021: Internal atmospheric variability of net surface heat flux in reanalyses and CMIP5 AMIP simulations. *Int. J. Climatol.*, 1–18, doi:10.1002/joc.7232.

Chelton, D. B., and S. P. Xie, 2015: Coupled ocean-atmosphere interaction at oceanic mesoscales. *Oceanography*, **23**(4), 52–69, https://doi.org/10.5670/oceanog.2010.05.

Cheng, L., K. E. Trenberth, J. Fasullo, T. Boyer, J. Abraham, and J. Zhu, 2017: Improved estimates of ocean heat content from 1960 to 2015. *Sci. Adv.*, **3**(3), e1601545. doi: 10.1126/sciadv.1601545.

Cheng, L., K. E. Trenberth, J. Fasullo, M. Mayer, M. Balmaseda, and J. Zhu, 2019: Evolution of ocean heat content related to ENSO. *J. Clim.*, **32**(12), 3529-3556, doi: 10.1175/JCLI-D-18-0607.1.

Cherchi, A., and Coauthors, 2019: Global mean climate and main patterns of variability in the CMCC-CM2 coupled model. *J. Adv. Model. Earth Syst.*, **11**(1), 185-209, doi: 10.1029/2018MS001369.

Condron, A., and I. A. Renfrew, 2013: The impact of polar mesoscale storms on northeast Atlantic Ocean circulation. *Nat.Geosci*., **6**, 34–37, doi:10.1038/ngeo1661.

Cronin, M. F., and Coauthors, 2019: Air-Sea Fluxes With a Focus on Heat and Momentum. *Frontiers in Marine Science*, **6**, 430, doi:10.3389/fmars.2019.00430.

Cuesta-Valero, F. J., A. García-García, H. Beltrami, J. F. González-Rouco, and E. García-Bustamante, 2021: Long-term global ground heat flux and continental heat storage from geothermal data. *Clim. Past*, **17**, 451–468, doi: 10.5194/cp-17-451-2021.

Danabasoglu, G., and Coauthors, 2020: The Community Earth System Model Version 2 (CESM2). *J. Adv. Model. Earth Syst.*, **12**(2), e2019MS001916, doi: 10.1029/2019MS001916.

Delworth, T., and R. Greatbatch, 2000: Multidecadal thermohaline circulation variability driven by atmospheric surface flux forcing. *Journal of Climate*, **13**, 1481–1495.

Demory, M. E., P. L. Vidale, M. J. Roberts, P. Berrisford, J. Strachan, R. Schiemann, and M. S. Mizielinski, 2014: The role of horizontal resolution in simulating drivers of the global hydrological cycle. *Clim. Dyn.*, **42**(7–8):2201–2225.

Dix, M., and Coauthors, 2019: CSIRO-ARCCSS ACCESS-CM2 model output prepared for CMIP6 CMIP AMIP. *Earth System Grid Federation*, doi: 10.22033/ESGF/CMIP6.4239.

Dong, B., and R. T. Sutton, 2002: Mechanism of interdecadal thermohaline circulation variability in a coupled ocean-atmosphere GCM. *Journal of Climate*, **18**, 1117–1135.

Donohoe, A., J. Marshall, D. Ferreira, and D. McGee, 2013: The relationship between ITCZ location and atmospheric heat transport across the equator: from the seasonal cycle to the last glacial maximum. *J. Clim.*, **26**(11), 3597–3618. doi:10.1175/JCLI-D-12-00467.1.

Eyring, V., and Coauthors, 2016: Overview of the Coupled Model Intercomparison Project Phase 6 (CMIP6) experimental design and organization. *Geoscientific Model Development*, **9(5)**, 1937–1958, doi:10.5194/gmd-9-1937-2016.

Frierson, D. M. W., and Y.-T. Hwang, 2012: Extratropical Influence on ITCZ Shifts in Slab Ocean Simulations of Global Warming. *J. Clim.*, **25** (2), 720–733, doi: 10.1175/JCLI-D-11-00116.1.

Ganachaud, A., and C. Wunsch, 2003: Large scale ocean heat and freshwater transports during the world ocean circulation experiment. *J. Clim.*, **16**(4), 696–705, doi: 10.1175/1520-0442(2003)016<0696:LSOHAF>2.0.CO;2.

Gelaro, R., and Coauthors, 2017: The Modern-Era Retrospective Analysis for Research and Applications, Version 2 (MERRA-2). *J. Clim.*, 30(14), 5419-5454, doi: 10.1175/JCLI-D-16-0758.1.

Haarsma, R. J., and Coauthors, 2016: High Resolution Model Intercomparison Project (HighResMIP v1.0) for CMIP6, *Geosci. Model Dev.*, **9**(11), 4185–4208, doi: 10.5194/gmd-9-4185-2016.

He, B., Y. Liu, G. Wu, and Coauthors, 2020: CAS FGOALS-f3-L model datasets for CMIP6 GMMIP Tier-1 and Tier-3 experiments. *Adv. Atmos. Sci.*, **37**(1), 18-28, doi: 10.1007/s00376-019-9085-y.

Hersbach, H., and Coauthors, 2020: The ERA5 global reanalysis. *Q. J. R. Meteorol. SOC.*, **146**(730), 1999–2049, doi: 10.1002/qj.3803.

Hirschi, J. J. M., B. Barnier, C. Böning, and Coauthors, 2020: The Atlantic meridional overturning circulation in high-resolution models. *J. Geophys. Res. Oceans*, **125**(4), e2019JC015522, doi: 10.1029/2019JC015522.

Holdsworth, A. M., and P. G. Myers, 2015: The influence of high frequency atmospheric forcing on the circulation and deep convection of the Labrador Sea. *J. Climate*, **28**, 4980–4996, doi:10.1175/JCLI-D-14-00564.1.

Hyder, P., J. Edwards, R. P. Allan, and Coauthors, 2018: Critical Southern Ocean climate model biases traced to atmospheric model cloud errors. *Nat. Commun.*, **9**, 3625, doi: 10.1038/s41467-018-05634-2.

Jansen, M. F., 2017: Glacial ocean circulation and stratification explainedby reduced atmospheric temperature. *PNAS*, **114**, 45-50, www.pnas.org/cgi/doi/10.1073/pnas.1610438113.

Johns, W. E., and Coauthors, 2011: Continuous, array-based estimates of Atlantic Ocean heat transport at 26.5° N. J Clim 24(10):2429–2449.

Josey, S. A., S. Gulev, and L. Yu, 2013: Exchanges through the ocean surface, *Ocean Circulation and Climate: A 21st Century Perspective*, G. Siedler et al., Eds, Academic Press, Oxford, 115–140.

Kang, S. M., Y. Shin, and S. P. Xie, 2018: Extratropical Forcing and Tropical Rainfall Distribution: Energetics Framework and Ocean Ekman Advection. *npj Clim. Atmos. Sci.*, **1**, 20172, doi: 10.1038/s41612-017-0004-6.

Kato, S., and Coauthors, 2013: Surface irradiances consistent with CERES-derived top-of-atmosphere shortwave and longwave irradiances. *J. Clim.*, **26**(9), 2719–2740. doi: 10.1175/JCLI-D-12-00436.1.

Kawai, H., S. Yukimoto, T. Koshiro, N. Oshima, T. Tanaka, H. Yoshimura, and R.Nagasawa, 2019: Significant improvement of cloud representation in the global climate model MRI-ESM2. *Geosci. Model Dev.,* **12**, 2875–2897, https://doi.org/10.5194/gmd-12-2875-2019.

Koenigk, T., and L. Brodeau, 2014: Ocean heat transport into the Arctic in the twentieth and twenty-first century in EC-Earth. *Clim. Dyn.*, **42**, 3101–3120. doi: 10.1007/s00382-013-1821-x.

Krishnan, R., and Coauthors, 2019: The IITM Earth System Model (ESM): Development and Future Roadmap, *Current Trends in the Representation of Physical Processes in Weather and Climate Models*, D. Randall, J. Srinivasan, R. Nanjundiah, and P. Mukhopadhyay, Eds, Springer Atmospheric Sciences. Springer, Singapore. doi: 10.1007/978-981-13-3396-5_9.

Kwon, Y.-O., and C. Frankignoul, 2012: Stochastically-driven multidecadal variability of the Atlantic meridional overturning circulation in CCSM3. *Climate Dynamics*, **38**, 859–976.

Lin, Y., X. Huang, Y. Liang, and Coauthors, 2020: Community Integrated Earth System Model (CIESM): Description and evaluation. *J. Adv. Model. Earth Syst.*, **12**(8), e2019MS002036, doi: 10.1029/2019MS002036.

Liang, X., and L. Yu, 2016: Variations of the Global Net Air-Sea Heat Flux During the "Hiatus" Period (2001-2010). *J. Clim.*, **29**(10), 3647-3660, doi:10.1175/JCLI-D-15-0626.1

Liu, C., R. P. Allan, P. Berrisford, M. Mayer, P. Hyder, N. G. Loeb, D. Smith, P. L. Vidale, and J. M. Edwards, 2015: Combining satellite observations and reanalysis energy transports to estimate global net surface energy fluxes 1985-2012. *J. Geophy. Res. Atmosphere,* **120**(18), 9374-9389*,* doi: 10.1002/2015JD023264

Liu, C., R. P. Allan, M. Mayer, P. Hyder, N. G. Loeb, C. D. Roberts, M. Valdivieso, J. M. Edwards, P.-L. Vidale, 2017: Evaluation of satellite and reanalysis-based global net surface energy flux and uncertainty estimates. *J. Geophy. Res. Atmosphere*, **122**(12), 6250-6272, doi: 10.1002/2017JD026616.

Liu, C., R. A. Allan, M. Mayer, P. Hyder, D. Desbruyères, L. Cheng, J. Xu, F. Xu, and Y. Zhang, 2020: Variability in the global energy budget and transports 1985-2017. *Clim. Dyn.,* **55**, 3381-3396*,* doi: 10.1007/s00382-020-05451-8.

Loeb, N. G, and Coauthors, 2012: Observed changes in top-of-atmosphere radiation and upper-ocean heating consistent within uncertainty. *Nat. Geosci.,* **5**, 110–113.

Loeb, N. G., H. Wang, A. Cheng, S. Kato, J. Fasullo, K. Xu, and R. P. Allan, 2016: Observational constraints on atmospheric and oceanic cross-equatorial heat transports: revisiting the precipitation asymmetry problem in climate models, *Clim. Dyn.,* **46**, 3239-3257, doi: 10.1007/s00382-015-2766-z.

Lumpkin, R., and K. Speer, 2007: Global ocean meridional overturning. *J. Phys. Oceanogr.,* **37**, 2550–2562, https ://doi.org/10.1175/JPO31 30.1.

Macdonald, A. M., 1998: The global ocean circulation: a hydrographic estimate and regional analysis. *Prog. Oceanogr*. **41**, 281–382.

Mayer, M., and L. Haimberger, 2012: Poleward Atmospheric Energy Transports and Their Variability as Evaluated from ECMWF Reanalysis Data. *J. Clim.*, **25**(2), 734–752, doi: 10.1175/JCLI-D-11-00202.1

Mayer, M., L. Haimberger, J. M. Edwards, and P. Hyder, 2017: Toward consistent diagnostics of the coupled atmosphere and ocean energy budgets. *J. Clim.*, **30**(22), 9225–9246, doi: 10.1175/JCLI-D-17-0137.1.

Mayer, J., M. Mayer, and L. Haimberger, 2021a: Consistency and Homogeneity of Atmospheric Energy, Moisture, and Mass Budgets in ERA5. *J. Clim.*, **34**(10), 3955-3974, doi: 10.1175/JCLI-D-20-0676.1.

Mayer, J., M. Mayer, L. Haimberger, and C. Liu, 2021b: Comparison of Surface Energy Fluxes from Global to Local Scale, submitted to *J. Climate*.

Mignac, D., D. Ferreira, and K. Haines, 2018: South Atlantic meridional transports from NEMO-based model simulations and reanalyses. *Ocean Science*, **14**, 53–68, doi: 10.5194/os-14-53-2018.

Moreno-Chamarro, E., and Coauthors, 2021: Impact of increased resolution on long-standing biases in HighResMIP-PRIMAVERA climate models. *Geoscientific model development*, https://doi.org/10.5194/gmd-2021-209.

Putrasahan, D. A., A. J. Miller, H. Seo, 2013: Isolating mesoscale coupled ocean–atmosphere interactions in the Kuroshio Extension region. *Dyn. Atmos. Oce.*, **63,** 60–78.

Rahmstorf, S., and A. Ganopolski, 1999: Long-term global warming scenarios computed with an efficient coupled climate model. *Climatic Change*, **43**, 353–367.

Roberts, M. J., H. T. Hewitt, P. Hyder, D. Ferreira, S. A. Josey, M. Mizielinski, and A. Shelly, 2016: Impact of ocean resolution on coupled air-sea fluxes and large-scale climate. *Geophy. Res. Lett.*, **43**(19), 10,430-10,438, doi: 10.1002/2016GL070559.

Roberts, M., 2017: MOHC HadGEM3-GC31-LL model output prepared for CMIP6 HighResMIP. https://doi.org/10.22033/ESGF/CMIP6.1901.

Roberts, C. D., M. D. Palmer, R. P. Allan, D. G. Desbruyeres, P. Hyder, C. Liu, and D. Smith, 2017: Surface flux and ocean heat transport convergence contributions to seasonal and interannual variations of ocean heat content. *J. Geophy. Res. Oceans*, **122**, 726–744, doi: 10.1002/2016JC012278.

Rong, X., 2019: CAMS CAMS-CSM1.0 model output prepared for CMIP6 ScenarioMIP. *Earth System Grid Federation*, doi: 10.22033/ESGF/CMIP6.11004.

Rong, X., 2020: CAMS CAMS-CSM1.0 model output prepared for CMIP6 HighResMIP. Earth System Grid Federation. doi: 10.22033/ESGF/CMIP6.11003 .

Sellar, A. A., C. G. Jones, J. P. Mulcahy, Y. Tang, A. Yool, A. Wiltshire, and Coauthors, 2019: UKESM1: Description and evaluation of the U.K. Earth System Model. *J. Adv. Model. Earth Syst.,* **11**, 4513-4558, doi: 10.1029/2019MS001739.

Senior, C. A., and Coauthors, 2016: Idealised climate change simulations with a high resolution physical model: HadGEM3-GC2. *J. Adv. Model. Earth Syst.*, **8**(2), 813-830, doi: 10.1002/2015MS000614.

Serreze, M. C., and R. G. Barry, 2011: Processes and impacts of Arctic amplification: a research synthesis. *Glob. Planet. Change.*, **77**, 85-96.

Smeed, D., and Coauthors, 2017: Atlantic meridional overturning circulation observed by the RAPID-MOCHA-WBTS (RAPID-Meridional Overturning Circulation and Heatflux Array-Western Boundary Time Series) array at 26N from 2004 to 2017. *Br.*

Oceanogr. Data Centre Nat. Environ. Res. Council UK. doi: 10.5285/5acfd 143-1104-7b58-e053-6c86a bc0d94b.

Swart, N. C., and Coauthors, 2019: The Canadian Earth System Model version 5 (CanESM5.0.3). *Geosci. Model Dev.*, **12**, 4823–4873, doi:10.5194/gmd-12-4823-2019.

Talley, L. D., 2003: Shallow, intermediate and deep overturning components of the global heat budget. *J. Phys. Oceanogr.,* **33**, 530–560.

Tatebe, H., and Coauthors, 2019: Description and basic evaluation of simulated mean state, internal variability, and climate sensitivity in MIROC6. *Geosci. Model Dev.*, **12**, 2727–2765, doi: 10.5194/gmd-12-2727-2019.

Terai, C. R., P. M. Caldwell, S. A. Klein, Q. Tang, M. L. Branstetter, 2018: The atmospheric hydrologic cycle in the ACME v0. 3 model. *Clim. Dyn.*, **50**(9–10), 3251–3279.

Trenberth, K. E., 1991: Climate Diagnostics from Global Analyses: Conservation of Mass in ECMWF Analyses. *J. Clim.*, **4**, 707–722, doi: 10.1175/1520-0442(1991)004<0707:CDFGAC>2.0.CO;2.

Trenberth, K. E., and A. Solomon, 1994: The global heat balance: heat transports in the atmosphere and ocean. *Clim. Dyn.*, **10**(3), 107–134, doi: 10.1007/BF00210625.

Trenberth, K. E., J. T. Fasullo, J. Kiehl, 2009: Earth's global energy budget. *Bull Am Meteorol Soc.* **90**, 311–323.

Trenberth, K. E., and J. T. Fasullo, 2017: Atlantic meridional heat transports computed from balancing Earth's energy locally. *Geophy. Res. Lett.*, **44**, 1919–1927, doi: 10.1002/2016GL072475.

Trenberth, K. E., and J. T. Fasullo, 2018: Applications of an updated atmospheric energetics formulation. *J. Clim.*, **31**, 6263–6279, doi: 10.1175/JCLI-D-17-0838.

Trenberth, K. E., Y. Zhang, J. T. Fasullo, and L. Cheng, 2019: Observation-Based Estimates of Global and Basin Ocean Meridional Heat Transport Time Series. *J. Clim.,* **32**, 4567-4583, doi: 10.1175/JCLI-D-18-0872.1.

Trenberth, K. E., and Y. Zhang, 2019: Observed interhemispheric meridional heat transports and the role of the Indonesian throughflow in the Pacific Ocean. J Clim 32:8523–8536, https ://doi.org/10.1175/JCLI-D-19-0465.1.

Uotila, P., H. Goosse, K. Haines, M. Chevallier, A. Barthélemy, C. Bricaud, and F. Kauker, 2019: An assessment of ten ocean reanalyses in the polar regions. *Clim. Dyn.,* **52**(3–4), 1613–1650.

Valdivieso, M., and Coauthors, 2015: An assessment of air-sea heat fluxes from ocean and coupled reanalyses. *Clim. Dyn.*, **49**, 983-1008, doi: 10.1007/s00382-015-2843-3.

Vanniere, B., and Coauthors, 2019: Multi-model evaluation of the sensitivity of the global energy budget and hydrological cycle to resolution. *Clim. Dyn.*, **52**(11), 6817-6846, ISSN 0930-7575 doi: https://doi.org/10.1007/s00382-018-4547-y.

Voldoire, A., and Coauthors, 2019: Evaluation of CMIP6 DECK experiments with CNRM-CM6-1, *J. Adv. Model. Earth Syst.*, **11**(7), 2177-2213, doi: 10.1029/2019MS001683.

Volodin, E., and A. Gritsun, 2018: Simulation of observed climate changes in 1850-2014 with climate model INM-CM5, *Earth Syst. Dynam.*, **9**, 1235–1242, doi: 10.5194/esd-9-1235-2018.

Volodin, E., and Coauthors, 2019: INM INM-CM5-H model output prepared for CMIP6 HighResMIP. *Earth System Grid Federation*. doi: 10.22033/ESGF/CMIP6.14041.

Von Schuckmann, K., and Coauthors, 2016: An imperative to monitor Earth's energy imbalance. *Nature Climate Change,* **6**, 138-144, doi: 10.1038/nclimate2876.

Von Schuckmann, K., and Coauthors, 2020: Heat stored in the Earth system: where does the energy go? *Earth Syst. Sci. Data*, 12, 2013-2041, doi: 10.5194/essd-12-2013-2020.

Williams, K. D., and Coauthors, 2015: The Met Office Global Coupled model 2.0 (GC2) configuration. *Geosci. Model Dev.*, **8**, 1509-1524, doi:10.5194/gmd-8-1509-2015.

Wong, T., and Coauthors, 2006: Reexamination of the observed decadal variability of the earth radiation budget using altitude-corrected ERBE/ERBS nonscanner WFOV data. *J. Clim.*, **19**(16), 4028–4040, doi: 10.1175/JCLI3838.1.

Wu, T., and Coauthors, 2019: The Beijing Climate Center Climate System Model (BCC-CSM): the main progress from CMIP5 to CMIP6 , *Geosci. Model Dev.*, **12**, 1573–1600, doi: 10.5194/gmd-12-1573-2019.

Wu, T., and Coauthors, 2021: BCC-CSM2-HR: a high-resolution version of the Beijing Climate Center Climate System Model. *Geosci. Model Dev.*, **14**, 2977–3006, doi: 10.5194/gmd-14-2977-2021.

Wu, Y., X. Zhai, and Z. Wang, 2017: Decadal impact of including ocean surface currents in bulk formulas on surface air-sea fluxes and ocean general circulation. *Journal of Climate*, 9511-9525.

Wu, Y, Z. Wang, and C. Liu, 2021: Impacts of Changed Ice-Ocean Stress on the North Atlantic Ocean: Role of Ocean Surface Currents. *Front. Mar. Sci.* **8**, 628892, doi: 10.3389/fmars.2021.628892.

Wu, Y., Z. M. Wang, C. Y. Liu, and X. Lin, 2020: Impacts of high-frequency atmospheric forcing on Southern Ocean circulation and Antarctic sea ice. *Adv. Atmos. Sci.*, **37**(5), 515-531.

Wu, Y., X. Zhai, and Z. Wang, 2016: Impact of synoptic atmospheric forcing on the mean ocean circulation. *J. of Climate*, **29**, 5709-5724.

Yu, L., and Coauthors, 2013: Towards achieving global closure of ocean heat and freshwater budgets: Recommendations for advancing research in air-sea fluxes through collaborative activities. Tech. rep., WCRP Informal/Series Report No. 13/2013.

Yu, L., and R. A. Weller, 2007: Objectively Analyzed Air–Sea Heat Fluxes for the Global Ice-Free Oceans (1981–2005). *Bulletin of the American Meteorological Society*, **88 (4)**, 527–540, doi:10.1175/BAMS-88-4-527

Zhao, M., and Coauthors, 2018a: The GFDL global atmosphere and land model AM4.0/LM4.0: 1. Simulation characteristics with prescribed SSTs. *J. Adv. Model. Earth Syst.*, **10**, 691–734, doi: 10.1002/2017MS001208.

Zhao, M., and Coauthors, 2018b: NOAA-GFDL GFDL-CM4C192 model output prepared for CMIP6 HighResMIP. *Earth System Grid Federation*, doi: 10.22033/ESGF/CMIP6.2262.

Ziehn, T., and Coauthors, 2020: The Australian Earth System Model: ACCESS-ESM1.5. *Journal of Southern Hemisphere Earth Systems Science*, **70**, 193–214, doi: 10.1071/ES19035.

Zuo, H., M. A. Balmaseda, S. Tietsche, K. Mogensen, and M. Mayer, 2019: The ECMWF operational ensemble reanalysis–analysis system for ocean and sea ice: a description of the system and assessment. *Ocean Sci.*, **15**(3), 779–808, doi: 10.5194/os-15-779-2019.

Table 1. Data sets and brief descriptions.

Data set	**Period (in this study)**	**Resolution**	**References**	Model number
DEEPC	1985-2017	0.7°×0.7°	Liu et al. (2020)	
RAPID	2004-2017		Smeed et al. (2017)	
ORAS5	1993-2016	0.25°×0.25°	Zuo et al. (2019)	
AMIP6	1985-2014			
ACCESS-CM2		1.25°×1.875°	Dix M et al. (2019)	1
ACCESS-ESM1-5		1.25°×1.875°	Ziehn T et al. (2020)	2
BCC-CSM2-MR		1.25°×1.875°	Wu et al. (2019)	3
CAMS-CSM1-0		1.125°×1.125°	Rong (2019)	4
CanESM5		2.81°×2.81°	**Swart et al. (2019)**	5
CESM2		0.94°×1.25°	Danabasoglu et al. (2020)	6
CIESM		0.94°×1.25°	Lin et al. (2020)	7
CMCC-CM2-SR5		0.94°×1.25°	Cherchi et al (2019)	8
CNRM-CM6-1		1.41°×1.41°	Voldoire et al. (2019)	9
CNRM_CM6_1_HR		0.5°×0.5°	Voldoire et al. (2019)	10
FGOALS-f3-L		1.0°×1.25°	He et al. (2020)	11
GFDL-AM4		1.0°×1.25°	Zhao et al. (2018a)	12
IITM-ESM		1.91°×1.875°	Krishnan R. et al. (2019)	13
INM-CM5-0		1.5°×2.0°	Volodin and Gritsun (2018)	14
IPSL-CM6A-LR		1.26°×2.5°	Boucher et al. (2019a)	15
MIROC6		1.41°×1. 41°	Tatebe et al. (2019)	16
MRI-ESM2-0		1.125°×1.125°	Kawai et al. (2019)	17
NESM3		1.875°×1.875°	Cao et al. (2018)	18
UKESM1-0-LL		1.25°×1.875°	Sellar et al. (2019)	19
highresSST-present	1985-2014			
BCC-CSM2-HR		0.45°×0.45°	Wu et al. (2021)	20
CAMS-CSM1-0		0.47°×0.46°	Rong (2020)	21
FGOALS-f3-H		0.25°×0.25°	Bao et al (2020)	22
FGOALS-f3-L		1. 25°×1.0°	Bao et al (2020)	23
GFDL-CM4C192		0.625°×0.5°	Zhao et al. (2018b)	24
INM-CM5-H		0.67°×0.5°	Volodin et al. (2019)	25
IPSL-CM6A-ATM-HR		0.7°×0.5°	Boucher et al. (2019b)	26
IPSL-CM6A-LR		2.5°×1.27°	Boucher et al. (2019c)	27

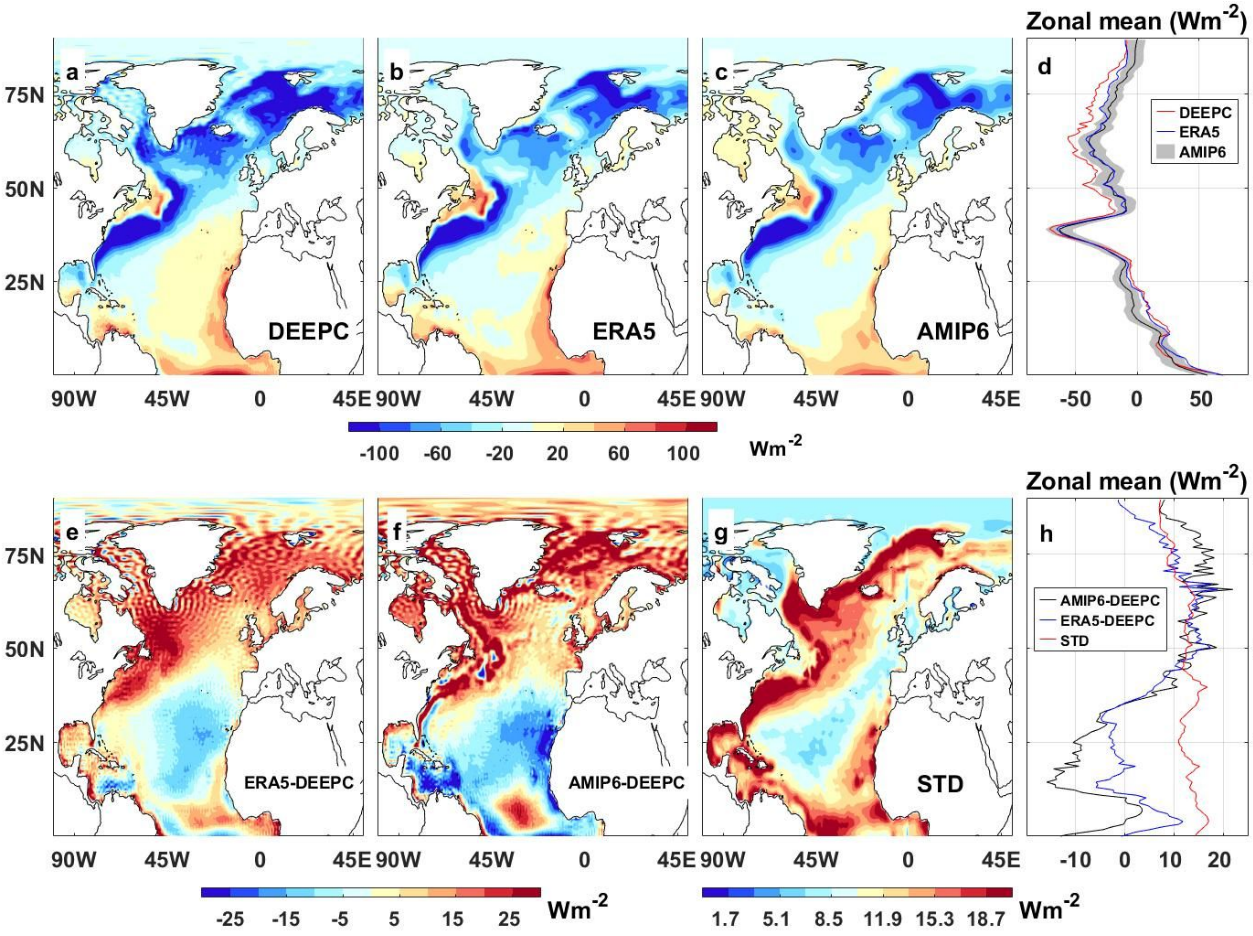

Fig. 1. Multiannual mean (2006-2013) of net surface fluxes from (a) DEEPC, (b) ERA5 and (c) AMIP6 (including *highresSST-present*), (d) is the corresponding zonal mean. Shaded area is the AMIP6 ensemble mean ± one standard deviation. Multiannual mean differences show (e) ERA5 minus DEEPC and (f) AMIP6 minus DEEPC. (g) is the standard deviation (STD) of AMIP6 and (h) is the corresponding zonal mean.

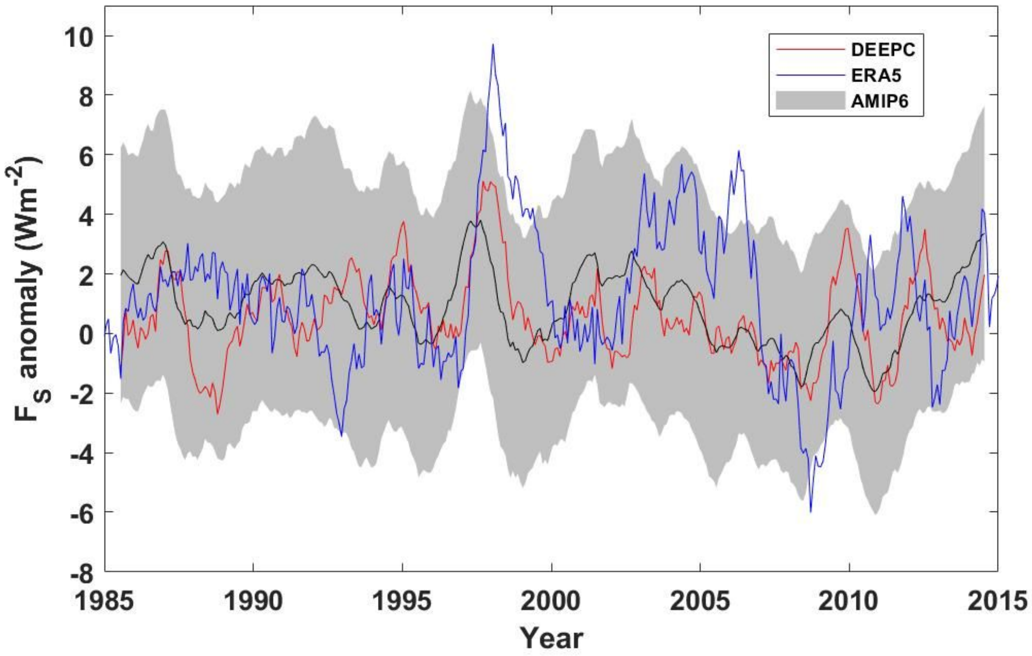

Fig. 2. Deseasonalized time series of the area mean ocean net surface heat flux north of 26°N in Atlantic. The shaded area is the AMIP6 ensemble mean (solid black line) ± one standard deviation. All lines are twelve-month running mean.

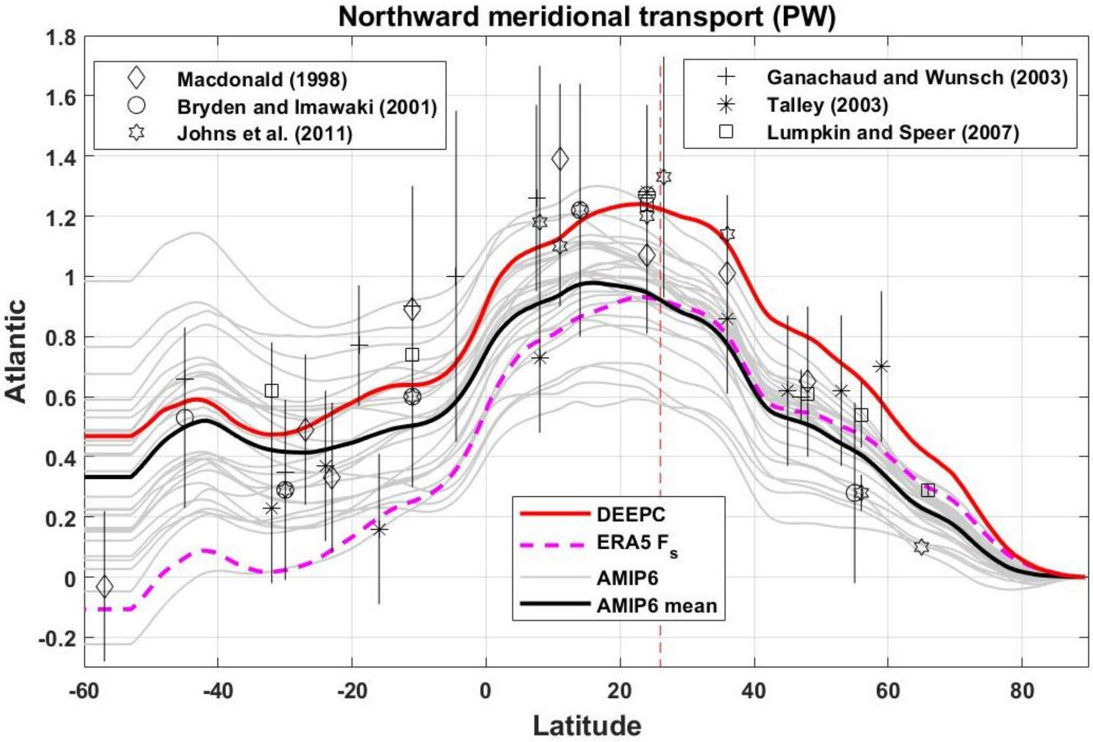

Fig. 3. Multiannual mean (2006–2013) northward total meridional oceanic heat transports (unit is PW) in Atlantic derived from net DEEPC surface fluxes, ORAS5 sea ice and OHCT, together with some short term historical observations (symbols, error bars show one standard deviation) and those inferred from ERA5 and AMIP6 model surface fluxes (including nineteen AMIP6 and eight *highresSST-present* model simulations). The vertical dashed red line shows the location of 26°N.

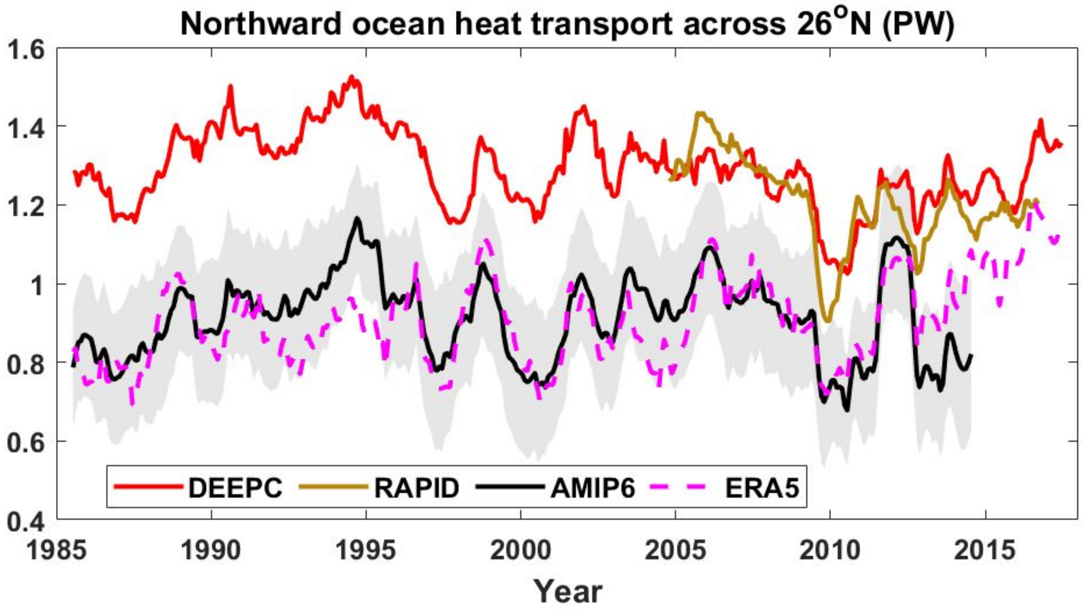

Fig. 4. Northward meridional ocean heat transports at 26°N of Atlantic from RAPID observations and DEEPC net surface fluxes taking into account the sea ice melting and ocean heat storage of ORAS5 0–2000 m, together with the transports inferred from ERA5 surface fluxes (dashed magenta). Grey shading is AMIP6 member mean ± one standard deviation. All lines are twelve-month running mean.

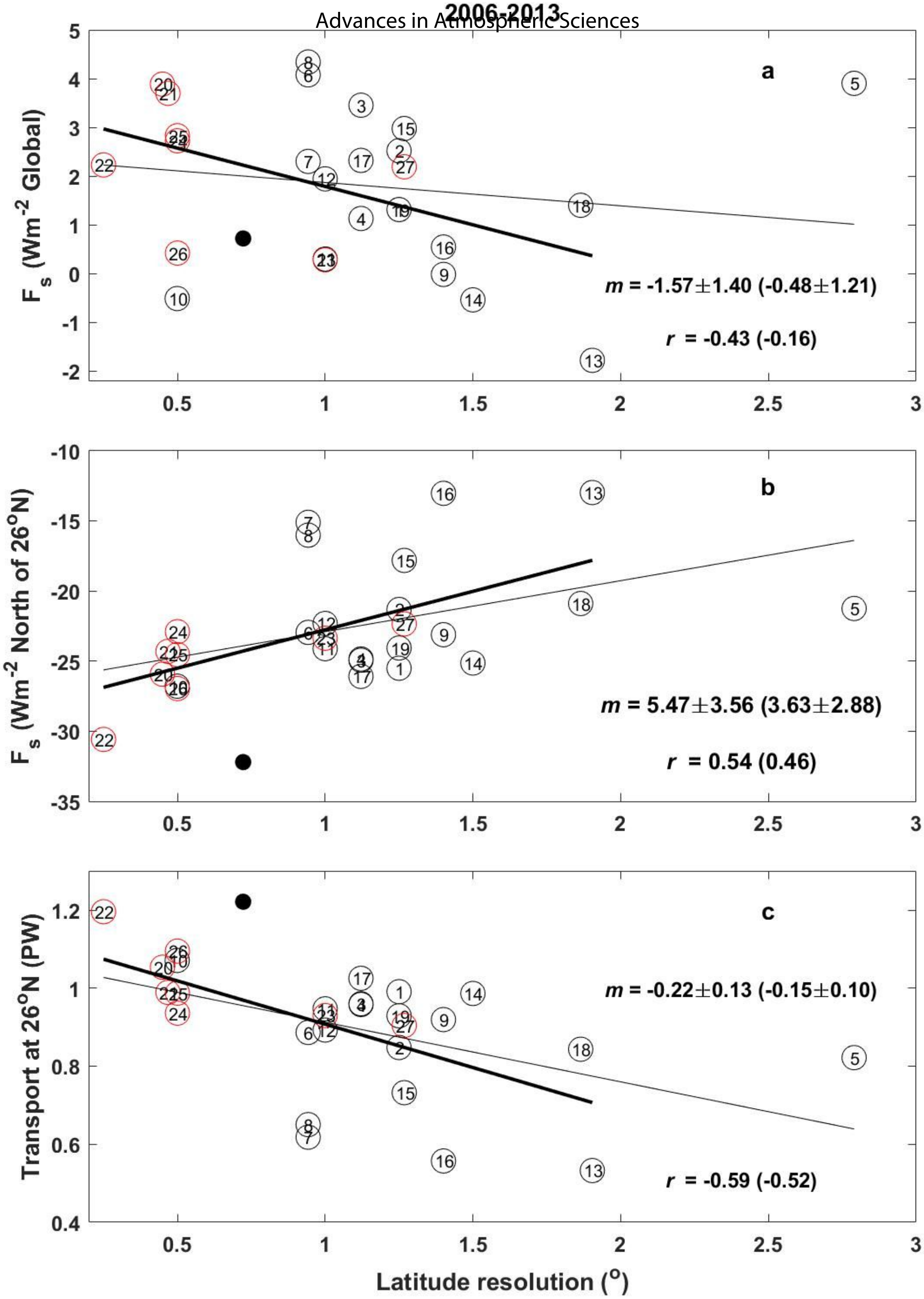

Fig. 5. Model resolution effect on multiannual mean (2006–2013) net surface flux over the (a) global and (b) the north of 26°N Atlantic. (c) is the effect on the oceanic heat transport at 26°N Atlantic. Circles with the number inside represent AMIP6 (red for highresSST) model simulations and the solid circle is from DEEPC. Correlation coefficients and the regression slopes are also displayed. The thin line and values in the bracket are with model 5 counted.

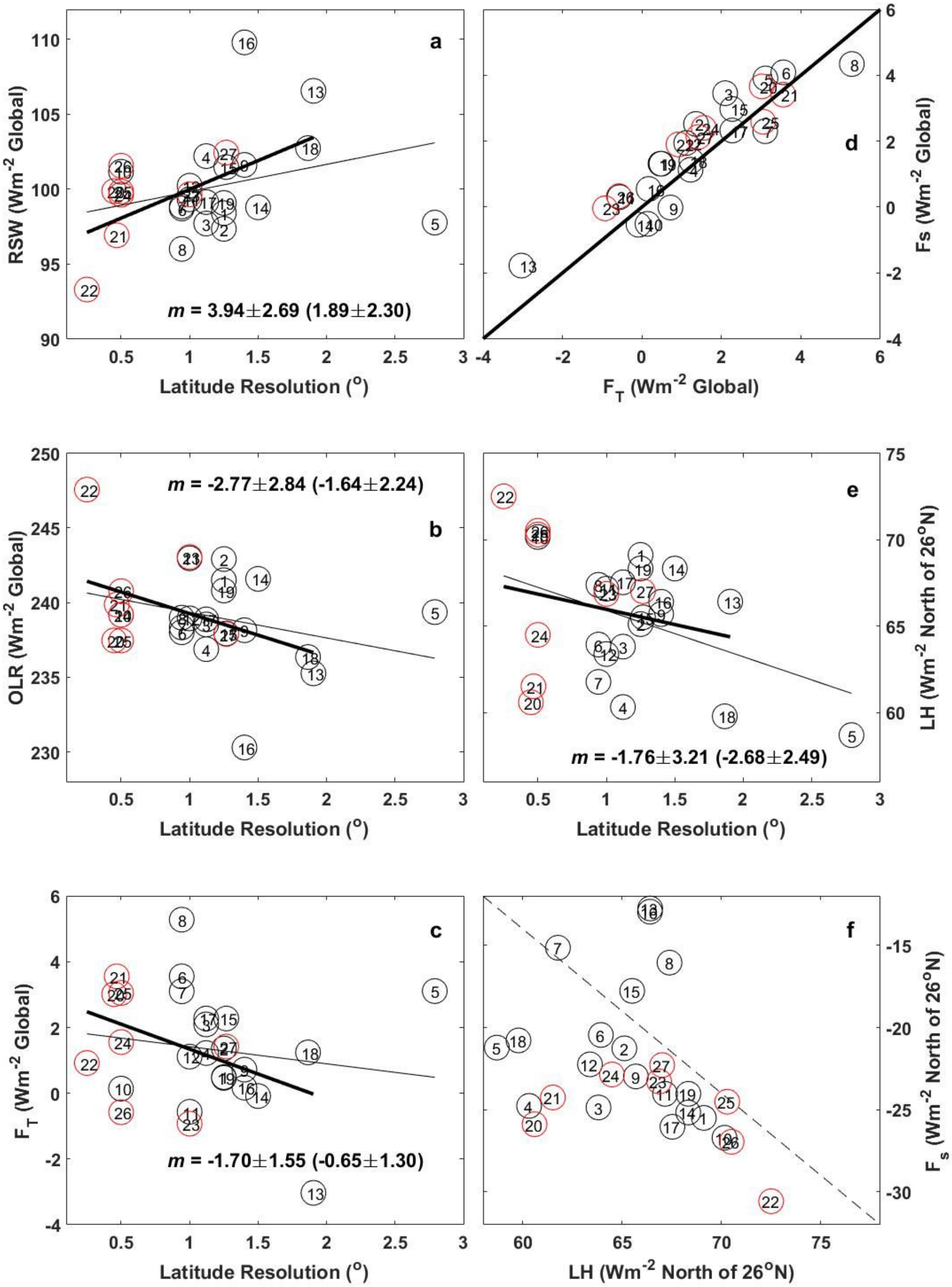

Fig. 6. Model resolution effect on multiannual (2006–2013) global mean (a) RSW, (b) OLR and (c) F_T. (e) is the LH over the north of 26°N Atlantic. (d) is the scatter plot between global mean F_T and F_S. (f) is the scatter plot between LH and F_S over the north of 26°N Atlantic. Model number is in the circle. The regression slopes are also displayed. The thin line and values in the bracket are with model 5 counted.